Linking the dielectric Debye process in 2-ethyl-1-hexanol to its density fluctuations.

Tina Hecksher[1]

[1] *Glass & Time, IMFUFA, Department of Sciences, Roskilde University, Postbox 260, DK-4000 Roskilde, Denmark*

(Dated: February 15, 2016)

We provide the first evidence that the puzzling dielectric Debye process observed in mono-alcohols is coupled to density fluctuations. The results open up for an explanation of the Debye process within the framework of conventional liquid-state theory. The spectral shape of dynamical bulk modulus of 2-ethyl-1-hexanol is nearly identical to that of the shear modulus, and thus the supramolecular structures believed to be responsible for the slow dielectric Debye process are manifested in the bulk modulus *in the same way* as in the shear modulus.

arXiv:1602.04196v1 [cond-mat.soft] 12 Feb 2016

All liquids can form a glass [1–8]. The most common route to the glassy state is through the supercooled liquid state where the liquid gradually becomes more and more viscous upon cooling and eventually falls out of equilibrium and forms a glass. Many viscous liquids display strikingly similar dynamical behavior regardless of their specific chemistry and this universality intrigues many physicists [1–8]. But although the field is old, the hallmark features of viscous liquids dynamics – non-Arrhenius temperature dependence of the viscosity and non-exponential relaxation – remain some of the major unsolved puzzles in condensed matter physics.

A class of liquids that do not conform to the general picture is the mono-alcohols. Mono-alcohols have become a hot topic in recent years (see the review by Böhmer *et al* [9]). Supercooled mono-alcohols differ from other viscous liquids in that the dominant process in the dielectric spectrum is: 1) Close to single-exponential rather following the stretched exponential form found in most viscous liquids [10–12]; mono-alcohols thus follow the prediction of Debye's theory [13], and the process is therefore often referred to as the "Debye-process". 2) Not associated with the structural glass transition [14–17], as is usually seen in viscous liquids where the kinetically defined glass transition temperature $\tau_\alpha(T_g) = 100$ s correlates well with the calorimetrically defined T_g. The faster process emerging on the high-frequency flank of the Debye process correlates much better with the structural glass transition and this process has accordingly been identified as the alpha process [14, 15, 18]. 3) Very intense. The Debye process is often so intense that it must originate from some structural correlation of several dipoles in the liquid. Dilution studies [19–22] and studies of structural isomers [23, 24] show that these characteristics may be less distinct, when the Debye process is not well-separated from the alpha process.

The notion that this intense dielectric signal originates from linear hydrogen-bonded structures appeared quite early [12, 25–27], and observations of a pre-peak in the static structure factor [28] supports this idea by identifying structures on a length scale exceeding the molecular. The different intensities of the Debye process in different mono-alcohols can be rationalized in terms of these structures being primarily chain-like – leading to a large end-to-end dipole moment – or ring-like – resulting in a (partial) cancellation of the individual dipole moments [12].

A number of mechanisms have been suggested to account for the slow dynamics of the Debye process: breaking of hydrogenbonds in a chain and formation of new chains leading to end-to-end fluctuations of the dipole moment [29–31], dipole inversion by rotation of the OH-groups [32], and the transient chain model advocated by Gainaru [33], where molecules break off from or add to the ends of the chain which promotes a slow rotation of the effective dipole moment of the chain. A fundamental and predictive model for the elusive Debye process is however still lacking. In particular, these models have nothing to say about whether or not this intense dielectric should be manifested in other types of responses. For years the consensus was that the Debye process is not linked to the mechanical or calorimetric responses, as summarized in 1997 by Hansen *et al*, the Debye process "possesses no counterpart signals in the quantities directly related to structural relaxation like viscosity and density fluctuations" [15]. Earlier shear modulus measurements seemed to confirm this picture [18]. However, there were some indications of a mechanical signature of the Debye process in ultrasonic measurements [31, 34], and it was recently established that the Debye process indeed has a weak shear mechanical counterpart [35]. The rheological response is similar to what is observed for short-chain polymers [24, 35–37]. The detection of a shear mechanical signature of the dielectric Debye process is difficult because the signal is small – especially compared to how dominant the dielectric signal is – and thus requires good resolution and accurate measurements.

A natural next step is to look for signatures in thermodynamic response functions. Could the dielectric Debye process in fact be coupled to the density fluctuations? This would open up a new route for modeling the Debye process. Density and density fluctuations are the central concepts in liquid state theory, where they define stan-

dard hydrodynamics [38], mode-coupling theory [39–41], and general density functional theory [42–44]. Moreover, density fluctuations provide a link to classical thermodynamics, where the state variables are scalar quantities such as pressure, volume, temperature and entropy. Both shear mechanics and dielectrics are non-scalar observables, and since a signature of the Debye process is thus far completely absent in the standard calorimetric scans, there is no established connection to thermodynamics.

Experimentally density fluctuations may be probed by measuring the volume response to a (linear) pressure perturbation. Recently, Dzida and Kaatze [45] published a study comparing the static adiabatic compressibility and the dielectric relaxation time of a range of mono-alcohols and showed how the concentration of hydrogenbonds affects the Debye relaxation time and the static compressibility differently at room temperature. But from this study no clear conclusions can be drawn about the dielectric Debye process' manifestation in the compressibility spectrum.

Here we present complex adiabatic bulk modulus data of the mono-alcohol 2-ethyl-1-hexanol (2E1H) measured over roughly four decades in frequency over a range of temperatures close to T_g. The adiabatic bulk modulus is defined as $K_S = V\,(\partial P/\partial V)_S$, i.e., the inverse of the compressibility. In addition, the complex shear modulus (G) was measured at the same temperatures and frequencies (spectra are shown in the Supplementary Material). Both bulk and shear modulus measurements were carried out in the same closed-cycle custom-built cryostat with the same measuring electronics [46, 47], ensuring identical experimental conditions. More details on the methods can be found in Refs. 48 and 49, and in the Supplementary Material.

The bulk modulus spectra are shown in Fig. 1. The frequency range of this measurement is from 2 Hz to 10 kHz. We clearly see the low-frequency liquid-like plateau at the high temperatures (red curves) and the high-frequency elastic plateau of the lower temperatures (blue curves) in the real part (Fig. 1(a)). The transition from low- to high-frequency plateau gives a peak in the imaginary part (Fig. 1(b)) as required by the Kramers-Krönig relations. The peak is the alpha relaxation peak, which moves down in frequency from around 10 kHz at 170 K to around 10 Hz at 154 K. At the lowest temperatures we see the onset of another peak (the beta relaxation) at the highest frequencies. The emergence of a secondary process is more evident in the master curve constructed in Fig. 1(c) by shifting each of the curves on the frequency axes to give the best overlap. The shift factors are shown in Fig. 1(d) together with the loss peak frequencies for the temperatures where the peak is inside the frequency window. There is excellent agreement between the two characteristic frequencies in the overlapping temperature region, thus confirming that the shifts made are reasonable.

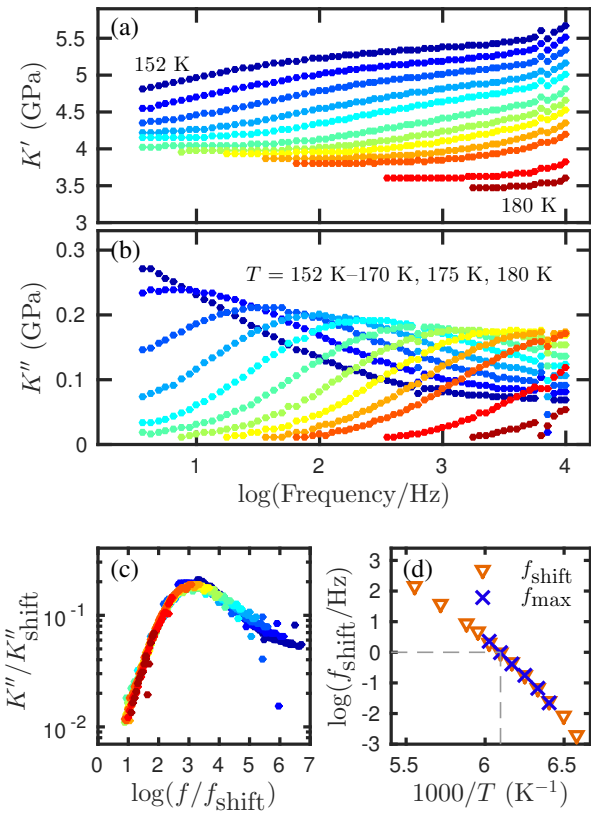

FIG. 1. Complex bulk modulus of 2E1H at several temperatures. (a) Real part of the bulk modulus. (b) Imaginary part of the bulk modulus. (c) Master curve of the imaginary part of the bulk modulus data on a logarithmic scale. The data are shifted on both axes to match the data at 164 K. (d) The shift factors as a function of inverse temperature showing a non-Arrhenius evolution of the characteristic time scale of the bulk modulus. The reference (164 K) is marked by the dashed lines. For comparison, we show the peak frequencies for the temperatures where the peak is in the frequency window, shifted to overlap at the reference temperature.

Figure 2 shows the imaginary parts of bulk modulus K (blue diamonds) and shear modulus G (yellow line) at the same temperature, 162 K. The shear modulus accurately reproduces the previously published results [35] shown in yellow circles. For comparison, the dielectric curve at 161.5 K from Ref. 18 is shown (red solid line). The dominant feature in the dielectric spectrum is the Debye process characteristic of mono-alcohols, where the alpha process is manifested as a high-frequency shoulder placed roughly where the alpha peak in the mechanical spectra appear. The recently established shear mechanical signature of the Debye process [35] shows up in the shear spectra as a deviation from the pure viscous behavior observed for non-associated liquids characterized by $G''(\omega) \propto \omega$ (unity slope in a double-logarithmic plot). The crossover from this intermedi-

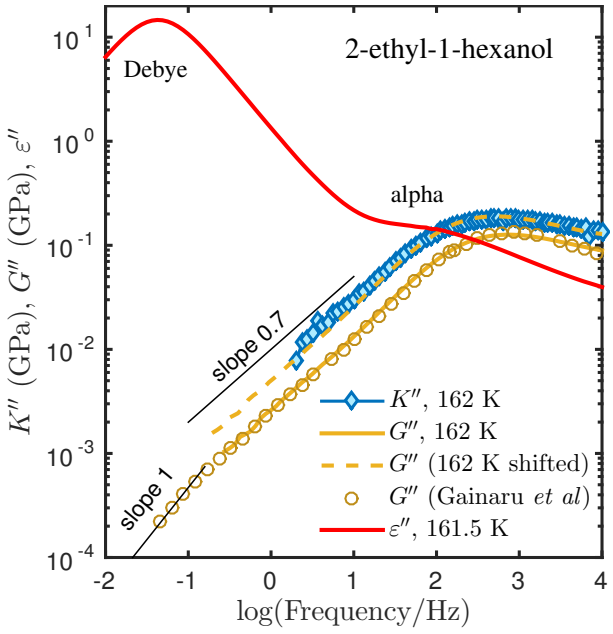

FIG. 2. Comparison of the imaginary parts of the bulk modulus (blue diamonds), shear modulus (solid yellow line), and dielectric constant (solid red line). Shear modulus is compared to the master curve presented in Ref. 35 (yellow circles) and reproduces the earlier data. The dielectric data at a matching temperature are from Ref. 18. The signature of the short-chain polymer like behavior is a slope < 1 on the low-frequency side of the shear modulus peak bending over to a purely viscous behavior (slope $= 1$) at ~ 0.1 Hz, corresponding roughly to the loss-peak frequency of the Debye peak in the dielectric spectrum. The bulk modulus curve follows the low-frequency behavior of the shear modulus accurately, but the crossover to purely viscous behavior is below the resolution limit of the bulk modulus measurement.

ate low-frequency power-law behavior with $G''(\omega) \propto \omega^{0.7}$ (slope 0.7 in a double-logarithmic plot) to the terminal viscous flow with $G''(\omega) \propto \omega$ behavior is located at a frequency close to the Debye peak frequency in the dielectric spectrum.

The shifted shear mechanical curve (yellow dashed line) shows that the bulk modulus displays the same deviation from pure viscous behavior as the shear modulus. Although the resolution of the bulk modulus measurement does not allow for showing a crossover to a pure viscous behavior, the bulk modulus in non-associated liquids typically displays a low-frequency purely viscous ($K'' \propto \omega$) behavior [50, 51]; hence a terminal purely viscous behavior is expected at frequencies and moduli below our current resolution limit.

To appreciate our findings it is important to give a few experimental details which is done in the following three paragraphs.

The technique used for measuring the dynamics bulk modulus is based on measuring the frequency-dependent capacitance of a piezo-electric spherical shell of 20 mm diameter – the Bulk Modulus Gauge (PBG) [48]. A picture of the PBG is shown as an inset of Fig. 3(a). When the PBG is empty it is free to deform in response to an applied voltage, and we measure a "free" capacitance. When the PBG is filled with a liquid, the liquid partially clamps the shell and, depending on the frequency, one measures a lower capacitance. The dynamic bulk modulus can then be inferred from the difference in capacitance between that of the freely moving shell and the partially clamped shell. The translation from a difference in capacitance to a bulk modulus of the liquid is somewhat involved, because the signal is mixed with the mechanical properties of the PBG itself and these effects needs to be disentangled. Furthermore, the small filling hole in the piezo-ceramic sphere leads to the liquid being able to flow *out* of the PBG at low frequencies. This is referred to as the "Helmholtz mode" [50] which gives an extra feature in the measured signal. Assuming that this flow can be described as a Poiseuille flow, we can treat it as a hydraulic resistance depending only on the shear viscosity of the liquid and compensate for the effect, making it possible to extend the frequency window of the bulk modulus measurement 0.5-1 decade. Details of this data extraction procedure is given in the Supplementary Material and in Refs. 48, 50, and 52.

In Fig. 3 the procedure is illustrated. The real part (Fig. 3(a)) of the uncorrected stiffness goes to zero at low frequencies, where the liquid flows in and out of the filling pipe and thus does not resist the deformation of the PBG (light blue, solid curve). This is the Helmholtz mode which in the imaginary part (Fig. 3(b)) appears as a prominent low frequency peak. The assumption of a purely viscous flow leads to a functional form (details are given in the Supplementary Material) of the peak shown in the imaginary part as a black dotted line and labelled "Helmholtz mode". The peak in the 2E1H data clearly has a shoulder in excess of this prediction, which when "subtracted" from the measured stiffness leaves a small peak (dark blue, dashed line). The inset of Fig. 3(b) shows that the prediction for a purely viscous flow holds and is easily "subtracted" from the stiffness for a non-associated, molecular liquid (data from Ref. 50).

The deviation from pure exponential behavior observed in the Helmholtz mode here can, however, be accounted for by inserting the measured *frequency-dependent* shear viscosity (defined as $\eta = G/(i\omega)$) instead of assuming a pure viscous flow. Then the true bulk modulus (blue circles) is revealed; this correction lifts the low-frequency real part to give a flat plateau and removes the spurious extra peak in the imaginary part. This fact provides clear and independent evidence that the low-frequency shear flow behavior of 2E1H differs both qualitatively and quantitatively from that of a non-associated liquid.

Compared to poly-alcohols the relaxation strength of

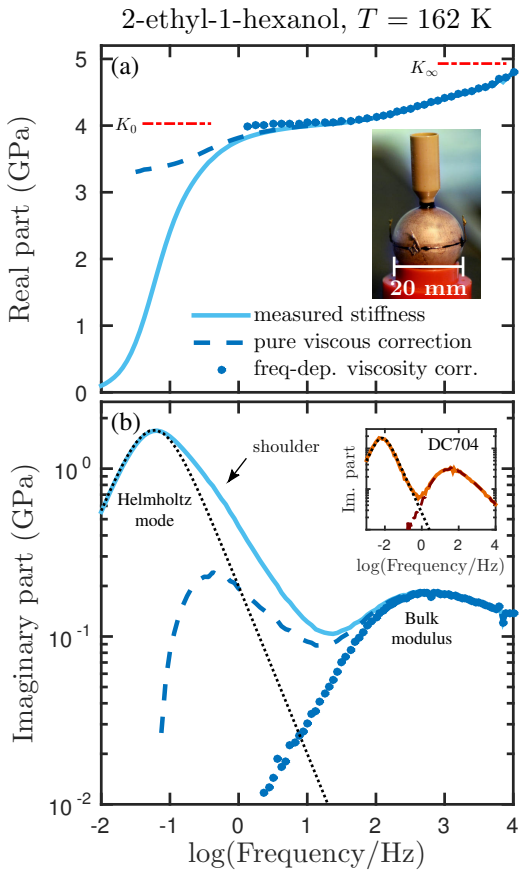

FIG. 3. Real (a) and imaginary (b) parts of the measured stiffness of 2E1H at 162 K. Inset of (a) is a picture of the measuring cell, the PBG [46, 48, 50]. At low frequencies, the real part of the measured stiffness goes to zero (light blue, solid line), because the liquid has time to flow in and out of the small filling tube. In the imaginary part, this is seen as a peak, denoted the Helmholtz mode. The simple, pure viscous correction is shown in both real and imaginary parts as the dashed blue line. It corresponds to "subtracting" the dotted black line in the imaginary part. While this procedure works perfectly in simple liquids, extending the frequency range of the bulk modulus by 0.5-1 decade (see inset of (b), where this is shown for DC704), it leads to an extra peak in the imaginary part and a corresponding extra step in the real part in the present case. The apparent extra process comes from the "shoulder" indicated by an arrow in the figure. The shoulder is consistent with the slow polymer-like frequency dependence of the low-frequency side of the shear viscosity in 2E1H recently documented [35] influencing the Poiseuille flow. Inserting the measured frequency-dependent shear modulus in the model (see Supplementary Materials) completely removes this shoulder and reveals the true bulk modulus (blue crosses).

the bulk modulus (and the shear modulus) of 2E1H is quite modest, roughly 1 GPa at the lowest temperatures. This relaxation strength is similar to what has been found for the shear modulus of other mono-alcohols, for instance *n*-propanol [53], 1-octanol and 2-octanol [54], and also what is typically found for the bulk and shear modulus of non-associated, molecular liquids [50, 51]. In glycerol [55] and propylene glycol [51, 56] the relaxation strength is a factor of four higher.

We speculate that this fact may be understood in terms of the type of molecular network formed in the poly-alcohols compared to the mono-alcohols. Poly-alcohols can form branched hydrogen-bonded networks which could lead to a stiffer structure and thus higher bulk and shear moduli. The mono-alcohols, on the other hand, primarily form linear structures (chains and/or rings). This presumably gives a "looser" structure, which is easier to deform and compress. The signature of these structures in the shear spectra is a subtle deviation from pure viscous behavior on the low-frequency side of the alpha peak, similar to that of a short-chain polymer [24, 35–37]. It is not trivial, however, that the bulk modulus of mono-alcohols deviates from that of non-associated liquids. The results presented here show that the bulk modulus displays the same low frequency behavior as the shear modulus, i.e., a non-trivial power law behavior at frequencies below the alpha relaxation peak. Thus the dielectric Debye process observed in mono-alcohols indeed does couple directly to the density fluctuations in the liquid. In my opinion, these findings open up for a less exotic explanation of the mysterious low-frequency Debye process, possibly based on conventional liquid state theory via density fluctuations.

The author thanks Bo Jakobsen and Tage Christensen for useful discussions and suggestions on the modeling and Jeppe Dyre for input to and feedback on the manuscript. This work was sponsored by the DNRF Grant no 61.

[1] W. Kauzmann, Chemical Review **43**, 219 (1948).
[2] G. W. Scherer, *Relaxation in Glass and Composites* (Wiley, New York, 1986).
[3] M. D. Ediger, C. A. Angell, and S. R. Nagel, J. Phys. Chem. **100**, 13200 (1996).
[4] C. A. Angell, K. L. Ngai, G. B. McKenna, P. F. McMillan, and S. W. Martin, J. Appl. Phys. **88**, 3113 (2000).
[5] P. G. Debenedetti and F. H. Stillinger, Nature **410**, 259 (2001).
[6] J. C. Dyre, Reviews of Modern Physics **78**, 953 (2006).
[7] M. D. Ediger and P. Harrowell, J. Chem. Phys. **137**, 080901 (2012).
[8] L. Berthier and M. Ediger, Physics Today **69**, 40 (2016).
[9] R. Böhmer, C. Gainaru, and R. Richert, Phys. Rep. **545**, 125 (2014).
[10] D. W. Davidson and R. H. Cole, J. Chem. Phys. **19**, 1484 (1951).
[11] R. H. Cole and D. W. Davidson, J. Chem. Phys. **20**, 1389 (1952).
[12] W. Dannhauser, J. Chem. Phys. **48**, 1911 (1968).
[13] P. Debye, *Polar Liquids* (The Chemical Catalog Company, Inc., New York, 1929).
[14] A. Kudlik, C. Tschirwitz, S. Benkhof, T. Blochowicz, and E. Rössler, Europhys. Lett. **40**, 649 (1997).

[15] C. Hansen, F. Stickel, T. Berger, R. Richert, and E. W. Fischer, J. Chem. Phys. **107**, 1086 (1997).
[16] L. M. Wang and R. Richert, J. Chem. Phys. **121**, 22 (2004).
[17] H. Huth, L.-M. Wang, C. Schick, and R. Richert, J. Chem. Phys. **126**, 104503 (2007).
[18] B. Jakobsen, C. Maggi, T. Christensen, and J. C. Dyre, J. Chem. Phys. **129**, 184502 (2008).
[19] S. Schwerdtfeger, F. Köhler, R. Pottel, and U. Kaatze, J. Chem. Phys. **115**, 4186 (2001).
[20] M. Preuss, C. Gainaru, T. Hecksher, S. Bauer, J. C. Dyre, R. Richert, and R. Böhmer, J. Chem. Phys. **137**, 144502 (2012).
[21] S. Bauer, H. Wittkamp, S. Schildmann, M. Frey, W. Hiller, T. Hecksher, C. G. N. B. Olsen, and R. Böhmer, J. Chem. Phys. **139**, 134503 (2013).
[22] Y. Gao, W. Tu, Z. Chen, Y. Tian, R. Liu, and L.-M. Wang, J. Chem. Phys. **139**, 164504 (2013).
[23] S. S. N. Murthy, J. Phys. Chem. **100**, 8508 (1996).
[24] T. Hecksher and B. Jakobsen, J. Chem. Phys. **141**, 101104 (2014).
[25] G. P. Johari and W. Dannhauser, J. Phys. Chem. **72**, 3273 (1968).
[26] M. A. Floriano and C. A. Angell, J. Chem. Phys. **91**, 2537 (1989).
[27] M. Iwahashi, Y. Hayashi, N. Hachiya, H. Matsuzawa, and H. Kobayashi, J. Chem. Soc. Faraday Trans. **89**, 707 (1993).
[28] D. Morineau and C. Alba-Simionesco, J. Chem. Phys. **109**, 8494 (1998).
[29] M. W. Sagal, J. Chem. Phys. **36**, 2437 (1962).
[30] O. E. Kalinovskaya and J. K. Vij, J. Chem. Phys. **112** (2000).
[31] U. Kaatze, R. Behrends, and R. Pottel, J. Non-Cryst. Solids **305**, 19 (2002).
[32] R. Minami, K. Itoh, H. Takahashi, and K. Higasi, Journal of Chemical Physics 73, 3396 (1980) **73**, 3396 (1980).
[33] C. Gainaru, Personal communication.
[34] R. Behrends and U. Kaatze, J. Phys. Chem. A **105**, 5829 (2001).
[35] C. Gainaru, R. Figuli, T. Hecksher, B. Jakobsen, J. C. Dyre, and M. A. B. Wilhelm, Phys. Rev. Lett. **112**, 098301 (2014).
[36] C. Gainaru, M. Wikarek, S. Pawlus, M. Paluch, R. Figuli, M. Wilhelm, T. Hecksher, B. Jakobsen, J. C. Dyre, and R. Böhmer, Colloid Polym. Sci. **292**, 1913 (2014).
[37] K. Adrjanowicz, B. Jakobsen, T. Hecksher, K. Kaminski, M. Dulski, M. Paluch, and K. Niss, J. Chem. Phys. **143**, 181102 (2015).
[38] J.-P. Hansen and I. R. McDonald, *Theory of simple liquids, 4th Ed.* (Elsevier, 2013).
[39] J. Bosse, W. Götze, and M. Lücke, Phys. Rev. A **17**, 434 (1978).
[40] W. Götze and L. Sjögren, Reports on Progess in Physics **55**, 241 (1992).
[41] S. P. Das, Rev. Mod. Phys. **76**, 785 (2004).
[42] R. Evans, Advances in Physics **28**, 143 (1979).
[43] Y. Rosenfeld, Phys. Rev. Lett. **63**, 980 (1989).
[44] R. Evans, "Fundamentals of inhomogeneous fluids," (Marcel Dekker, 1992) Chap. Density Functionals in the Theory of Nonuniform Fluids, pp. 85–176.
[45] M. Dzida and U. Kaatze, J. Phys. Chem. B **119**, 12480 (2015).
[46] B. Igarashi, T. Christensen, E. H. Larsen, N. B. Olsen, I. H. Pedersen, T. Rasmussen, and J. C. Dyre, Rev. Sci. Instrum. **79**, 045105 (2008).
[47] B. Igarashi, T. Christensen, E. H. Larsen, N. B. Olsen, I. H. Pedersen, T. Rasmussen, and J. C. Dyre, Rev. Sci. Instrum. **79**, 045106 (2008).
[48] T. Christensen and N. B. Olsen, Phys. Rev. B **49**, 15396 (1994).
[49] T. Christensen and N. B. Olsen, Rev. Sci. Instrum. **66**, 5019 (1995).
[50] T. Hecksher, N. B. Olsen, K. A. Nelson, J. C. Dyre, and T. Christensen, J. Chem. Phys. **138**, 12A543 (2013).
[51] D. Gundermann, K. Niss, T. Christensen, J. C. Dyre, and T. Hecksher, J. Chem. Phys. **140**, 244508 (2014).
[52] T. Hecksher, *Relaxation in supercooled liquids.*, Ph.D. thesis, Roskilde University (2010).
[53] R. Kono, T. A. Litovitz, and G. E. McDuffe, J. Chem. Phys. **45**, 1790 (1966).
[54] F. Palombo, P. Sassi, M. Paolantoni, A. Morresi, and R. S. Cataliotti, J. Phys. Chem. B **110**, 18017 (2006).
[55] C. Klieber, T. Hecksher, T. Pezeril, D. H. Torchinsky, J. C. Dyre, and K. A. Nelson, J. Chem. Phys. **138**, 12A544 (2013).
[56] C. Maggi, B. Jakobsen, T. Christensen, N. B. Olsen, and J. C. Dyre, J. Phys. Chem. B **112**, 16320 (2008).

Supplementary Material: Linking the dielectric Debye process in 2-ethyl-1-hexanol to its density fluctuations.

EXPERIMENTAL DETAILS

The sample, 2-ethyl-1-hexanol (2E1H), was purchased from Sigma-Aldrich (purity $\geq$ 99.6 %) and used as received.

All bulk and shear modulus measurements were carried out in the same experimental set-up, at the same temperatures (however, the shear modulus measurement included some lower temperatures than the bulk modulus measurement) and frequencies.

The set-up includes a custom-built closed-cycle cryostat able to keep the temperature stable within about 1 mK. The temperature calibration procedure benchmarks absolute temperature stability to better than 0.1 K, however the actual absolute temperature stability may be slightly worse, because it depends on temperature gradients in the cryostat, i.e., the thermal contact between sample cell and the stick, and the thermal contact between the stick and the inner walls of the cryostat chamber. This can vary between different types of cells (due to slightly different positions in the cryostat, difference in masses and/or materials) and from measurement to measurement (due to different handling).

The electronics of the set-up consist of a custom-built generator for frequencies up to 100 Hz, a HP 3458A multimeter (measuring at low frequencies) and an Agilent E4980A Precision LCR meter (measuring frequencies up to 2 MHz).

Further details of the experimental set-up is given in Refs. S1 and S2. Details of measuring techniques in given Ref. S3 (shear modulus technique) and Refs. S4 and S5 (bulk modulus technique).

SHEAR MECHANICAL DATA

Shear modulus data for 2E1H was published in Refs. S6 and S7, but rather than using the old data we decided to measure again. This was done for several reasons: 1) previous measurements were carried out at slightly different temperatures 2) measurements were performed in a different experimental set-up 3) it was a "cleaner" implementation when data points are at exactly the same frequencies (as in the bulk modulus measurement) instead of shifting a master curve in frequency and then interpolating between frequencies to match the bulk modulus measurement.

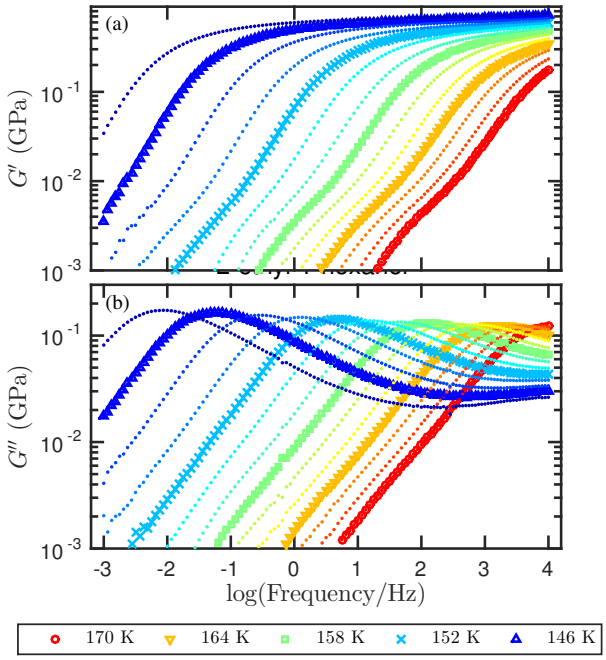

FIG. S1. Real (a) and imaginary (b) part of the shear modulus of 2E1H at temperatures from 170 K to 144 K in steps of 2 K.

Shear modulus was thus re-measured in the same experimental set-up as the bulk modulus, changing only the measuring cell while the cryostat, cryostat stick, and electronics were identical under the two measurements. Data

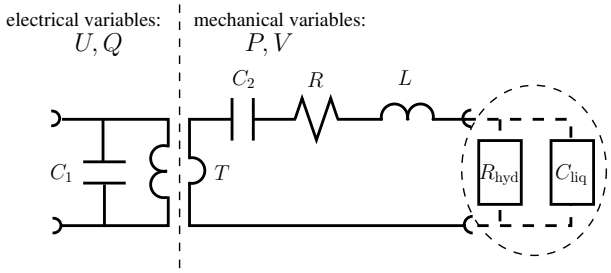

FIG. S2. Model of the PBG. The transformer (also marked by a vertical dashed line) separates the electrical and the mechanical side of the model. The encircled area shows the part that is only present when the PBG is filled. An empty transducer corresponds to the mechanical port of the model being shorted. The electrical side (left of the transformer, T) the capacitance C_1 models the electrical capacitance of the piezo-electric ceramic shell. On the mechanical side (right of the transformer) the RCL-circuit models the mechanical properties of the ceramics. The transformer models the piezo-electric conversion of the applied electrical field to mechanical displacement. When there is liquid in the PBG, there is an extra (complex) capacitance due to the liquid (C_{liq}), and an extra (complex) resistor (R_{hyd}) modeling the flow in the filling pipe.

are shown in Fig. S1. The data agree well with previously published shear modulus data [S6, S7] for 2E1H.

MODEL FOR THE PBG

This section gives the background for the data treatment of the bulk modulus data and is essential to the conclusions drawn.

The PBG can be modeled by an electrical diagram, where each element represents a particular property of the PBG [S5]. Such a diagram is essentially a simple way of constructing the constitutive equations of the PBG in a physically consistent manner.

Figure S2 shows the electrical diagram model of the PBG. The model has an electrical side (left) and a mechanical side (right) where the volume V plays the role of electrical charge Q and the pressure P is the equivalent of the voltage U on the electrical side. The transformer (separating the two sides of the diagram) represents the piezo-electric conversion of electrical voltage to a mechanical displacement. The capacitance on the electrical side C_1 models the electrical capacitance of the piezo-electric ceramic shell. On the mechanical side, the RCL-circuit models the mechanical properties of the ceramics. When there is liquid in the transducer, an extra (complex) capacitance due to the liquid (C_{liq}), and an extra (complex) resistor (R_{hyd}) modeling the flow in the filling pipe is added to the model.

Using the simple rules for adding electrical network elements (impedances added in series, admittances added in parallel), we arrive at the following expression for the measured capacitance, i.e., the response when measured at the electrical side of the model

$$C_{\mathrm{m}}(\omega) = C_1 + T^2 \frac{1}{\frac{1}{C_2} + i\omega R - \omega^2 L + \left[\frac{1}{\frac{1}{i\omega R_h} + C_{\mathrm{liq}}}\right]}\,, \tag{S1}$$

where the expression in the square brackets only is present if the PBG is filled with liquid.

Equation (S1) can be rewritten in some convenient variables: the clamped (high-frequency limit) capacitance $C_{cl} = C_1$, the free (low-frequency limit) capacitance $C_{fr} = C_1 + T^2 C_2$, the resonance frequency $\omega_0 = \sqrt{1/LC_2}$, and the quality factor $Q = 1/R\sqrt{L/C_2}$. The rewritten expression is then

$$C_{\mathrm{m}}(\omega) = C_{cl} + \frac{C_{fr} - C_{cl}}{1 + i\frac{\omega}{\omega_0}\frac{1}{Q} - \frac{\omega^2}{\omega_0^2} + \left[\frac{C_2}{\frac{1}{i\omega R_{\mathrm{hyd}}} + C_{\mathrm{liq}}}\right]}\,. \tag{S2}$$

The hydrodynamic flow resistance R_{hyd} is proportional to the shear viscosity, η_G. Assuming a Poiseuille flow (see Sec. below), the factor of proportionality is given by

$$A = \frac{8L}{\pi a^4}\,, \tag{S3}$$

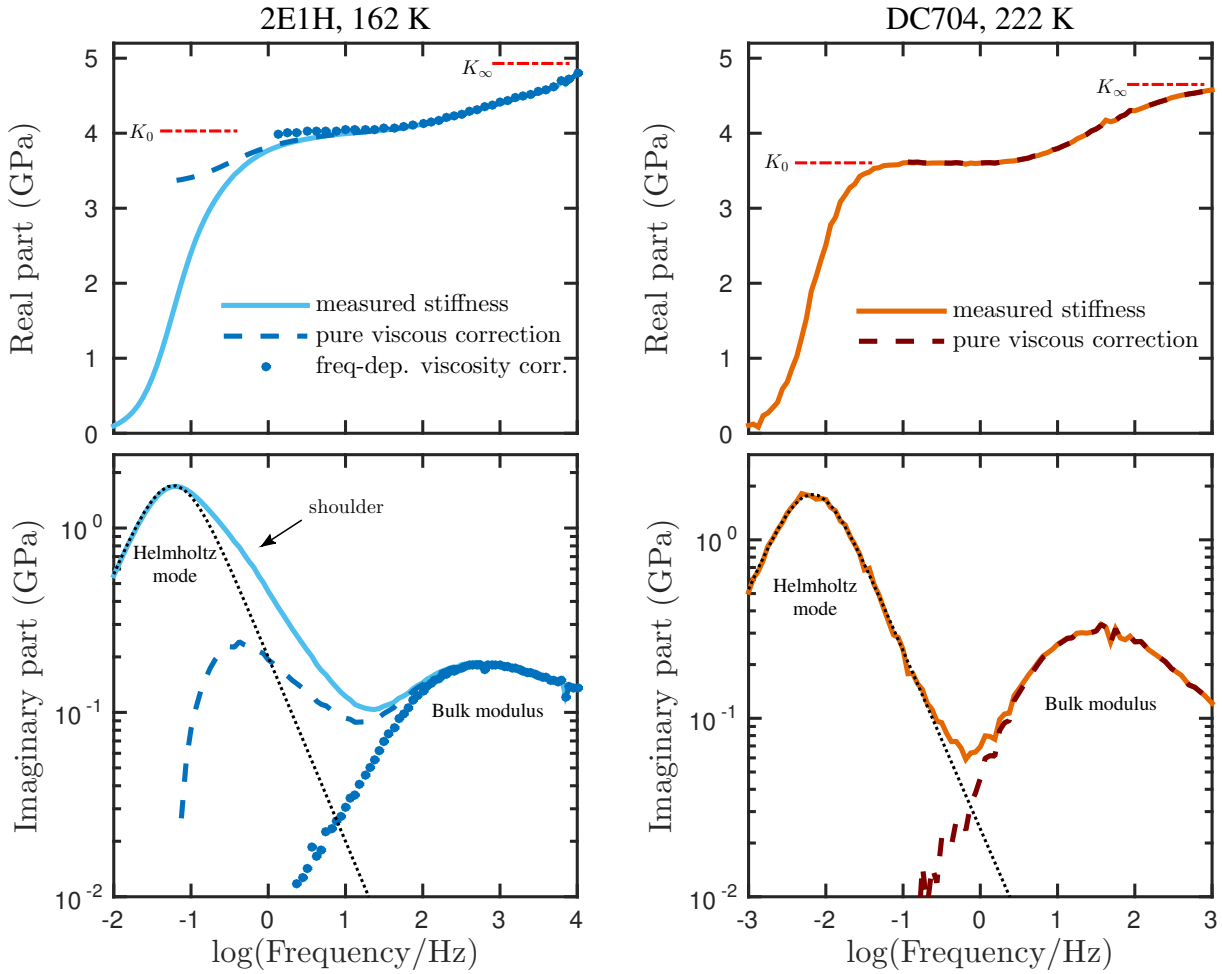

FIG. S3. Real and imaginary parts of the measured stiffness of 2-ethyl-1-hexanol (2E1H) and the silicone oil, tetraphenyl-tetramethyl-trisiloxane (DC704). At low frequencies, the real part of the measured stiffness goes to zero (solid line), because the liquid has time to flow in and out of the small filling tube and thus there is no resistance to the deformation of the piezo-ceramic shell. In the imaginary part this is seen as a peak, the Helmholtz mode. In the real part the limiting low- and high-frequency moduli, K_0 and K_∞ are indicated by red dashed lines. The simple, purely viscous correction (see Eq. (S1)) is shown in both real and imaginary parts as the dashed line. It corresponds to the "subtraction" of the dotted black line in the imaginary part. While this procedure works perfectly in non-associated molecular liquids, extending the frequency range of the bulk modulus by approximately 1 decade (shown here for DC704), it clearly leads to an extra peak in the imaginary part and a corresponding extra step in the real part in the case of 2E1H. This apparent extra process comes from the "shoulder" indicated by an arrow in the imaginary part of the 2E1H spectrum. The shoulder is consistent with the slow polymer-like frequency dependence of the shear viscosity in 2E1H recently documented [S7] influencing the Poiseuille flow. Inserting the measured frequency-dependent shear modulus in the model (Eq. (S5)) completely removes this shoulder and reveals the true bulk modulus (blue crosses).

where L is the length of the pipe and a is the radius. Inserting this and rearranging Eq. (S2) to isolate $C_{\rm liq}$ (which is the signal we are after), we arrive at

$$C_{\rm liq}(\omega) = C_2 \left(F^{-1} - 1 - i\frac{\omega}{\omega_0}\frac{1}{Q} + \frac{\omega^2}{\omega_0^2} \right)^{-1} - \frac{1}{i\omega A \eta_G} \tag{S4}$$

where $F = \frac{C_{\rm m}(\omega) - C_{cl}}{C_{fr} - C_{cl}}$.

For liquids that display a "simple" low-frequency behavior in the shear modulus (e.g., most non-associated molecular liquids), it is sufficient to plug in the DC viscosity in the model (corresponding to a pure resistor in the network in place of the $R_{\rm hyd}$-box in Fig. S2). A more sophisticated model takes the frequency-dependence of the viscosity into account. This could either be done by putting in a more complicated model for $R_{\rm hyd}$, but one could also plug in the

actual measured shear viscosity. Since $\eta_G = \frac{G}{i\omega}$, where G is the complex shear modulus we finally arrive at

$$C_{\rm liq}(\omega) = C_2 \left(F^{-1} - 1 - i\frac{\omega}{\omega_0}\frac{1}{Q} + \frac{\omega^2}{\omega_0^2} \right)^{-1} - \frac{1}{AG} \,. \tag{S5}$$

The bulk modulus (with the "subtracted" hydrodynamic flow in the filling pipe) is obtained as follows

$$K_S(\omega) = \frac{V}{C_{\rm liq}(\omega)} \,, \tag{S6}$$

where $C_{\rm liq}$ is given by Eq. (S5).

The procedure is illustrated in Fig. S3, where both the pure viscous correction and the correction including the frequency-dependence of the viscosity is shown for 2E1H. For comparison, we show how the pure viscous correction works for a non-associated molecular liquid, the commercial silicone oil DC704 [S5].

COMMENTS ON THE POISEUILLE FLOW ASSUMPTION

In fluid dynamics, the Poiseuille law relates the flowrate, $\dot{V}$ to the pressure drop δP over the pipe

$$\dot{V} = R_{\rm hyd} \delta P \,, \tag{S7}$$

where the hydrodynamic resistance $R_{\rm hyd}$ inversely proportional to the fluid's viscosity, η. The constant of proportionality is the geometrical constant given by Eq. (S3).

The assumptions of Eq. (S7) are that 1) the liquid is incompressible and Newtonian, 2) the flow is laminar, 3) there is no acceleration of fluid in the pipe and 4) the pipe has constant circular cross-section and the length of the pipe is substantially longer than its radius.

In our case we do not have a constant flow, but a pulsating flow where the frequency of the pulsations varies from 1 mHz to 10 kHz. Of course assumption of zero acceleration no longer holds, but the requirement of a laminar flow translates into the frequency of pulsations being sufficiently low so that a parabolic velocity profile has time to develop during each cycle. In that case the Poiseuille equation hold to a good approximation. This is fulfilled when Womersley number, α, is small. Wormersley number is given by

$$\alpha = a\sqrt{\frac{\omega\rho}{\eta(\omega)}} \,. \tag{S8}$$

where ω is the angular frequency, ρ is the density, η is the frequency-dependent viscosity and a is the radius of the pipe.

In Fig. S4 the Womersley number is shown as a function of frequency and temperature in the case of 2E1H and clearly shows that $|\alpha| < 1$ at all temperature in the relevant frequency range, and thus assumptions two and three are met.

The filling pipe is cylindrical, the radius is approximately $a \approx 1.5$ mm, while the length is approximately $L \approx 4$ mm. The requirement that $a/L \ll 1$ is maybe not completely met. However, when in a pulsating flow the problem is smaller at high frequencies. In agreement with this, we observe that the correction building on the Poiseuille flow assumption gradualy breaks down for low frequencies (i.e., for frequencies lower than the peak frequency of the Helmholtz mode, see Fig. S3).

The Poiseuille equation has been shown to work (surprisingly) well for supercooled molecular liquids at the frequency ranges and pipe dimensions explored here [S5].

DETERMINING THE GEOMETRIC FACTOR

The geometric factor in Eq. (S3) that enters the calculation of the Poiseuille flow correction consist of the length, L, and diameter, a, of the filling tube. In principle, these quantities can be determined by measuring directly the dimension of the tube. In practice, this is not so easy since the filling tube is hidden at the bottom of a larger liquid reservoir, and so it is difficult measure the tiny dimensions accurately inside measuring cell.

Instead we 'calibrate' the geometrical constant with another set of shear and bulk modulus data measured in the same experimental set up, and – in the case of the bulk modulus – in the same measuring cell. In Fig. S5 we show

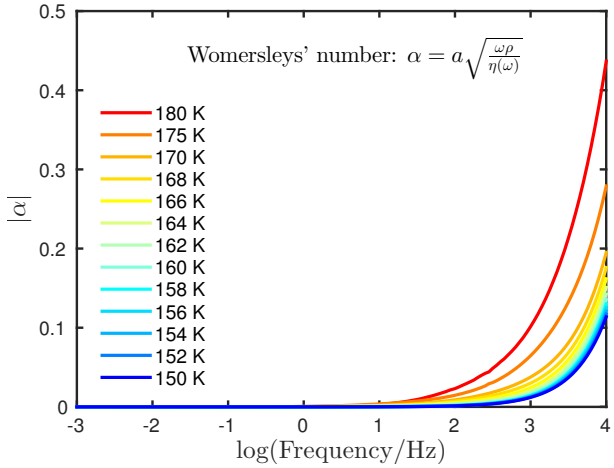

FIG. S4. Womersley number calculated as a function of frequency for 2E1H at several temperatures. When α is small (< 1), it means the frequency of pulsations is sufficiently low that a parabolic velocity profile has time to develop during each cycle, and the flow will be very nearly in phase with the pressure gradient. The flow will then be given by Poiseuille's law to a good approximation, using the instantaneous pressure gradient.

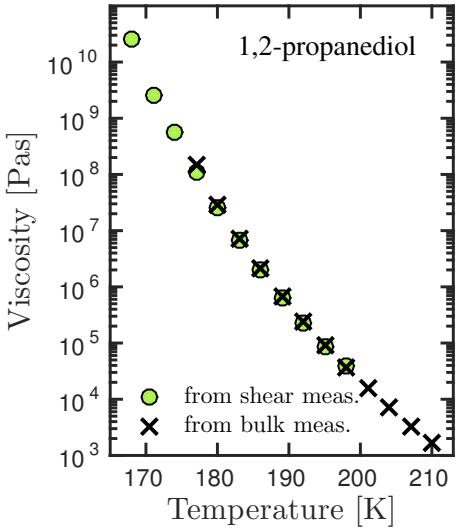

FIG. S5. Shearviscosity of 1,2-propanediol measured directly as the low-frequency plateau of the real part of the complex shearviscoity, $\eta = G/i\omega$, and as inferred from the Poiseuille flow in the bulk transducer described in the text (for more details, see Ref. [S5]). Data are from Ref. [S8]. This determines the geometric factor of the translation between hydraulic resistance and shear viscosity for that particular transducer (named q10 for internal reference) to $A = 3.6 \times 10^9$ m^{-3}.

the static shear viscosity as determined from the low-frequency plateau value of the frequency-dependent viscosity measured in the PSG (green circles) as well as the static shear viscosity determined by the Helmholtz mode [S5] with a geometric factor adjusted, so the two curves coincide. The geometric factor used for correcting the low-frequency side of the bulk modulus spectra was $A = 3.6 \times 10^9$ m^{-3}. This values agrees qualitatively with the number found when inserting the values for radius and length stated in Sec. above in Eq. (S3).

[S1] B. Igarashi, T. Christensen, E. H. Larsen, N. B. Olsen, I. H. Pedersen, T. Rasmussen, and J. C. Dyre, Rev. Sci. Instrum. **79**, 045105 (2008).
[S2] B. Igarashi, T. Christensen, E. H. Larsen, N. B. Olsen, I. H. Pedersen, T. Rasmussen, and J. C. Dyre, Rev. Sci. Instrum. **79**, 045106 (2008).
[S3] T. Christensen and N. B. Olsen, Rev. Sci. Instrum. **66**, 5019 (1995).

[S4] T. Christensen and N. B. Olsen, Phys. Rev. B **49**, 15396 (1994).
[S5] T. Hecksher, N. B. Olsen, K. A. Nelson, J. C. Dyre, and T. Christensen, J. Chem. Phys. **138**, 12A543 (2013).
[S6] B. Jakobsen, C. Maggi, T. Christensen, and J. C. Dyre, J. Chem. Phys. **129**, 184502 (2008).
[S7] C. Gainaru, R. Figuli, T. Hecksher, B. Jakobsen, J. C. Dyre, and M. A. B. Wilhelm, Phys. Rev. Lett. **112**, 098301 (2014).
[S8] D. Gundermann, K. Niss, T. Christensen, J. C. Dyre, and T. Hecksher, J. Chem. Phys. **140**, 244508 (2014).